Palmitoyl piperidinopiperidine, a novel derivative of 10-hydroxy-2-decenoic acid, as a potent and selective anticancer agent against human colon carcinoma cell lines

SAEKO ANDO[1], KATSUMI FUKAMACHI[1], ERI YOSHIMOTO[1], HARUTOSHI MATSUMOTO[1,2], MUNEKAZU IINUMA[3] and MASUMI SUZUI[1]

Departments of [1]Neurotoxicology and [2]Clinical Pharmacy, Graduate School of Medical Sciences and Medical School, Nagoya City University, Nagoya, Aichi 467-8601; [3]Laboratory of Pharmacognosy, Gifu Pharmaceutical University, Gifu 501-1196, Japan

Received February 1, 2020; Accepted October 20, 2020

DOI: 10.3892/ijo.2020.5160

Abstract. The present study, to the best of our knowledge, is the first systematic study of the inhibitory effects of palmitoyl piperidinopiperidine (PPI; Japan Patent no. 5597427), on colon carcinogenesis. PPI exhibited marked growth inhibitory activity in several human colon carcinoma cell lines, with IC_{50} values of approximately 0.5-2.2 μM. *In silico* docking analysis indicated that PPI could bind to the SH2 domain of signal transducer and activator of transcription 3 (STAT3). PPI markedly inhibited the transcriptional activity of the SW837 cell line. Flowcytometric analysis demonstrated that PPI induced an increase in the number of cells in the G1 phase of the cell cycle, and induced sub-G1 fractions of cells at a higher concentration level of PPI. In the HT29 and SW837 cells, western blot analyses exhibited that in whole cell lysates, PPI induced a marked decrease in the expression levels of p-STAT3, but not in the levels of STAT3 in these cells. PPI also induced a marked decrease in the expression levels of both STAT3 and p-STAT3 in the chromatin fraction. In addition, PPI affected the protein expression levels of cyclin D1, p53, Bcl-2, Bcl-xL and vascular endothelial growth factor (VEGF). In the HT29 cells, PPI induced a marked and dose-dependent increase in the expression levels of Bax, cleaved caspase-3, cleaved caspase-7, cleaved caspase-8, cleaved caspase-9 and cleaved poly (ADP-ribose) polymerase (PARP). In animal model systems, PPI inhibited the growth of implanted carcinoma cells, and also induced a significant decrease in the multiplicity of colonic aberrant crypt foci. In addition, a marked and dose-dependent inhibition of angiogenesis of the chick chorioallantoic membrane was observed. As regards the possible molecular mechanisms, it is suggested that the inhibition of STAT3 by PPI may affect the function of molecules that are related to apoptosis, angiogenesis and cell cycle progression, eventually contributing to the PPI-induced growth inhibitory effects.

Correspondence to: Professor Masumi Suzui, Department of Neurotoxicology, Graduate School of Medical Sciences and Medical School, Nagoya City University, 1 Kawasumi, Mizuho-cho, Mizuho-ku, Nagoya, Aichi 467-8601, Japan
E-mail: suzui@med.nagoya-cu.ac.jp

Key words: anticancer activity, palmitoyl piperidinopiperidine, colon carcinoma, apoptosis, cell cycle control, signal transducer and activator of transcription 3, tumor xenograft assay, aberrant crypt foci

Introduction

There is increasing interest in the use of natural products for treatment and/or prevention of a variety of diseases (1,2). Natural products, such as propolis processed by honeybees, contain a wide variety of chemical compounds that exert potent biological effects, and also exhibit anticancer activity (3). The authors have previously the growth inhibitory activity of ethanol extracts from plant resin-derived propolis in human colon carcinoma cell lines (3). The authors have also previously found that the dietary administration of powdered leaves of *Peucedanum japonicum* and *Terminalia catappa* reduces the occurrence of azoxymethane-induced aberrant crypt foci (ACF), preneoplastic lesions in rat colon carcinogenesis (4,5).

The medium-chain fatty acid (FA), 10-hydroxy-2-decenoic acid (10-HDA) (Fig. 1A), is the most abundant FA and a major lipid component of the honeybee product, royal jelly (RJ) (6,7). This unique FA exhibits a broad range of biological and pharmacological properties (8-10). For instance, there are several studies reporting the antibacterial activity of RJ against Gram-positive and Gram-negative bacteria (6,11-13). However, limited experimental evidence is available for the biological properties, including the anticancer and anti-inflammatory activities of 10-HDA (14,15).

In the present study, inspired by the biological profile of 10-HDA in continuation of a previous study (16) by the authors, a novel compound, 1-palmitoyl-4-piperidinopiperidine (PPI), that exhibits a resemblance to 10-HDA in its backbone structure, was synthesized. The aim of the present study was to examine the anticancer activities of PPI. In addition, the present

study aimed to elucidate the molecular mechanisms through which it inhibits the growth of human colon carcinoma cells, focusing on the possibility that it may exert its effects, at least in part, by suppressing the function of a signal transducer and activator of transcription 3 (STAT3) and its related molecules.

Materials and methods

Chemistry and chemicals. PPI (Fig. 1B) was synthesized by the authors (17). In brief, palmitic acid and 1-hydroxybenzotriazole were dissolved in dimethylformamide, and 4-piperidinopiperidine was added and mixed (solution 1). 1-Ethyl-3-(3-dimethylaminopropyl)-carbodiimide was dissolved in dimethylformamide (solution 2). Solutions 1 and 2 were mixed under cooled conditions (4˚C) for 2 h and at room temperature for 12 h. Chloroform was added to the reaction product and followed by washing with hydrochloric acid twice and saturated brine solution twice.

Cryptotanshinone (CTS) (Tokyo Chemical Industry Co., Ltd.), a specific inhibitor of the signal transducer and activator of transcription 3 (STAT3) SH2 domain, and 5-fluorouracil (5-FU; Sigma-Aldrich; Merck KGaA) were dissolved in dimethyl sulfoxide (DMSO; Sigma-Aldrich; Merck KGaA). All chemicals were stored at -20˚C until use.

Silica gel column chromatography. The remaining chloroform solution was purified with silica gel column chromatography, yielding PPI. PPI (=1-(1,4'-bipiperidin-1'-yl)hexadecan-1-one): Mp. 189˚C; EIMS *m/z* (rel. int.): 406 $[M]^+$ (42), 377 (12), 322 (11), 167 (46), 124 (100), 110 (20), 84 (30); ^{1}H-NMR (400 MHz, $CDCl_3$) δ: 0.88 (3H, t, *J*=6.8 Hz), 1.25 (26H, br s), 1.60-1.69 (5H, m), 2.00-3.40 (4H, br s), 2.17 (2H, m), 2.30 (2H, dd, *J*=8.8, 7.8 Hz), 2.53 (2H, m), 3.08 (2H, m), 3.26 (2H, m), 4.01 (1H, m), 4.86 (1H, m). PPI was dissolved in acetone (FUJIFILM Wako Pure Chemical Corp.).

Cells and cell culture. HT29, SW480, SW837 and HCT116 human colorectal carcinoma cell lines, and the FHC human colon normal epithelial cell line were obtained from the American Type Culture Collection (ATCC). Exponentially dividing cells were maintained in Dulbecco's modified Eagle's medium (DMEM; FUJIFILM Wako Pure Chemical Corporation) supplemented with 10% (v/v) fetal bovine serum (BioWest S.A.S.) in an incubator with humidified air at 37˚C with 5% CO_2. Cells were plated in 10-cm culture dishes (Thermo Fisher Scientific, Inc.), treated with 1.0-10 μM PPI for 24 or 48 h and harvested. As an untreated vehicle control, cells were treated with acetone or DMSO at a final concentration ≤0.5%.

Cell proliferation assays. Cell viability was determined using colony formation and MTT assays performed as previously described (18). Carcinoma cells were plated into 6-well 35-mm-diameter culture plates ($7.5x10^2$ cells/well) and treated with 0.3% acetone (control) or various concentrations (0.25-5 μM) of PPI for 7 days in DMEM plus 10% FBS. After washing with phosphate-buffered saline (PBS), colonies were fixed with 100% methanol (FUJIFILM Wako Pure Chemical Corporation) and stained with Giemsa solution at room temperature for 30 min (Sigma-Aldrich; Merck KGaA) and then counted.

Carcinoma cells or colon normal epithelial cells were seeded into 96 well plates ($1-5x10^3$ cells/well). Cells were treated with acetone/DMSO (control) or increasing concentrations of 0.07-12.5 μM PPI, 1.2-20 μM CTS or 1.2-20 μM 5-FU for 48 or 96 h. MTT reagent (50 μg) was added to each well, and assayed using an MTT assay kit (Roche Diagnostics GmbH). The absorbance was measured at 595 nm using a spectrophotometric microplate reader (Model 680 series microplate readers; Bio-Rad Laboratories, Inc.). The IC_{50} value was calculated from kinetic parameters derived from the growth curve data of each chemical. All assays were performed in duplicate or triplicate and yielded similar results. In these two assay systems, the relative surviving fraction, when compared with cells treated with the vehicle, was plotted on the dose-response curve. A viability of 100% corresponds to the control cells.

Flow cytometric analysis. Flow cytometric analysis was performed as previously described (19). The HT29 and SW837 cells were plated onto 10-cm dishes in DMEM containing 10% FBS. After synchronizing the cells with serum starvation, the cells were treated with 0.1% acetone (control) or 1-10 μM PPI for 48 h, harvested, fixed with 70% ethanol, centrifuged (750 x g for 5 min at room temperature), resuspended in 400 μl of PBS containing 2 mg/ml RNase (Nacalai Tesque Inc., Kyoto, Japan), and stained with 400 μl of 0.1 mg/ml propidium iodide (Nacalai Tesque, Inc.). The cell suspension was filtered through a 40 μm nylon filter (Ikemoto Scientific Technology Co. Ltd.). Samples of 20,000 cells were then analyzed for DNA histograms and cell cycle phase distributions by flowcytometry using a FACSCalibur instrument (BD Biosciences), and the data were analyzed by a CELLQuest computer program (BD Biosciences), as previously described (20).

Detection of apoptosis. In cell cultures, apoptosis was detected by observing DNA fragmentation on agarose gel electrophoresis as previously described (19). In brief, following treatment of the HT29 cells with 10 μM PPI for 48 h, the cells were harvested, centrifuged (750 x g for 5 min at room temperature) and washed twice with PBS. The cell pellet was then homogenized in 50 mM SEDTA (0.1 M NaCl and 50 mM EDTA). Following supplementation with 1% sodium dodecyl sulfate (SDS), the homogenate was digested with proteinase K (FUJIFILM Wako Pure Chemical Corporation) and extracted twice with phenol/chloroform, and DNA was precipitated with ethanol. Following RNase treatment, DNA fragmentation was visualized by agarose gel electrophoresis and ethidium bromide (0.5 μg/ml) staining. Apoptosis was also detected by flow cytometric analysis as described above.

Transient transfection reporter assays. Reporter assays were performed as previously described (18). The SW837 cells were plated into 6-well 35-mm-diameter culture plates ($5x10^4$ cells/well) in DMEM plus 10% FBS and cultured overnight to allow for cell attachment. Subsequently, 1 μg of STAT3 Luciferase Reporter Vector (Panomics, Inc.) was transiently transfected into the cells using Lipofectamine 3000 transfection reagent (Thermo Fisher Scientific, Inc.). Following transfection (approximately 24 h), the cells were

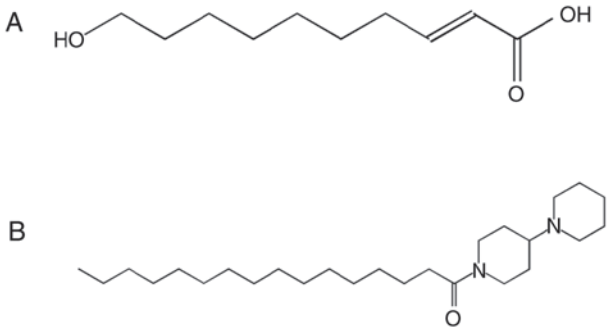

Figure 1. Chemical structures of (A) 10-hydroxy-2-decenoic acid (10-HDA, $C_{10}H_{18}O_3$, MW186) and (B) palmitoyl piperidinopiperidine (PPI, $C_{26}H_{50}N_2O$, MW406.6).

incubated with 0.5% acetone (control) or 0.6-2.5 μM PPI in DMEM plus 10% FBS for 24 h. Cell extracts were then prepared, each sample was assayed in triplicate using a luciferase assay system (Promega Corp.), and luciferase activity was measured using a TD-20/20 Luminometer (Promega Corp.). A CMV-driven β-galactosidase expression plasmid (Promega Corp.) was co-transfected into the cells to normalize the transfection efficiency.

Preparation of whole-cell lysates. Whole-cell lysates were prepared according to previously established procedures (21). The HT29 and SW837 cells were treated with 0.5% acetone (control) or 1.0-10 μM PPI for 24-48 h and harvested. The cells were then lysed with modified radioimmunoprecipitation assay (RIPA) buffer [150 mM NaCl, 1% NP40, 0.1% SDS, 50 mM Tris-HCl (pH 8.0), 0.5% deoxycholic acid, 2 mM EDTA, 2 mM EGTA, 1 mM DTT, and 25% glycerol].

Preparation of cytosolic and chromatin fractions. The HT29 and SW837 cells ($6.5x10^5$ cells/10-cm diameter dish) were treated with 0.1% acetone (control) or 1.2-2.5 μM PPI for 24 h, harvested and resuspended in solution A (10 mM HEPES pH 7.9, 10 mM KCl, 1.5 mM $MgCl_2$, 11% sucrose, 10% glycerol, 0.1% Triton X, 1 mM DTT, 0.1 mM Na_3VO_4, 10 mM NaF, 20 μg/ml aprotinin, 20 μg/ml leupeptin and 20 μM PMSF). The cytoplasmic fraction was separated from the nuclei by centrifugation (1,300 x g for 4 min, 4˚C). Isolated nuclei were lysed in solution B (3 mM EDTA, 0.2 mM EGTA, 1 mM DTT, 20 μg/ml aprotinin, 20 μg/ml leupeptin and 20 μM PMSF). The chromatin fraction was separated from the nuclei by centrifugation (1,700 x g for 4 min, 4˚C). Cytoplasmic and chromatin fractions were subjected to SDS-PAGE (12% gel) and examined by western blot analysis.

Western blot analysis. The assay was performed according to previously established procedures using Bio-Rad Protein Assay Dye Reagent Concentration (Bio-Rad Laboratories, Inc.) (21). The whole-cell lysate, cytosolic fractions and chromatin fractions (20-80 μg protein per lane) were separated by SDS-PAGE (12.0-13.5% gel) and transferred onto an Immobilon-P transfer membrane (EMD Millipore). The membranes were then blocked at room temperature for 1 h with 3% BSA in TBS-T [50 mM Tris-HCl (pH 7.5), 150 mM NaCl, and 0.2% Tween-20], followed by incubation at room temperature for 1 h with primary antibodies to β-actin (sc-1616R, Santa Cruz Biotechnology, Inc., 1:200), histone H3 (ab1791, Abcam, 1:1,000), caspase-3 (sc-65497, Santa Cruz Biotechnology, Inc., 1:200), caspase-7 (sc-6138, Santa Cruz Biotechnology, Inc., 1:200), caspase-8 p18 (sc-7890, Santa Cruz Biotechnology, Inc., 1:200), caspase-9 p10 (sc-7885, Santa Cruz Biotechnology, Inc., 1:200), poly (ADP-ribose) polymerase (PARP; #9542, Cell Signaling Technology, Inc., 1:1,000), STAT3 (sc-7179, Santa Cruz Biotechnology, Inc., 1:200), phosphorylated (p)-STAT3 (Tyr705) (#9131, Cell Signaling Technology, Inc., 1:1,000), cyclin D1 (06-137, EMD Millipore, 1:1,000), p53 (sc-126, Santa Cruz Biotechnology, Inc., 1:200), Bcl-2 (sc-509, Santa Cruz Biotechnology, Inc., 1:200), Bcl-xL (sc-8392, Santa Cruz Biotechnology, Inc., 1:200), Bax (sc-526, Santa Cruz Biotechnology, Inc., 1:200) and vascular endothelial growth factor (VEGF; sc-7269, Santa Cruz Biotechnology, Inc., 1:200). The membranes were then incubated at room temperature for 1 h with secondary antibodies (anti-mouse IgG, NA931, Cytiva, 1:4,000 or anti-rabbit IgG, NA934, Cytiva, 1:3,000) and each band was visualized with a Light-CaptureII imaging analyzer (ATTO Corp.).

Molecular docking analysis. Computational work was performed using Discovery Studio 2017R2 (Dassault Systèmes BIOVIA software programe, BIOVIA). For calculation, the CHARMm force field was applied and the CDOCKER algorithm was used to dock PPI into the protein. Using the CDOCKER protocol, the binding affinity was evaluated by the -CDOCKER_ENERGY (kcal/mol) obtained from the docking analysis of a compound of interest. The crystal structure of the target protein was obtained from RCSB Protein data bank (PDB) (https://www.rcsb.org/). The PDB code of STAT3 was 3CWG. The structure of PPI was sketched in ChemDraw computer program (PerkinElmer, Inc.).

Chick chorioallantoic membrane (CAM) assays. A modified CAM assay was performed to clearly visualize blood vessels. PPI was dissolved in 1.0% methylcellulose solution (methylcellulose is dissolved in PBS). As an untreated vehicle control, acetone was added to the 1.0% methylcellulose solution at a final concentration ≤0.5%. The fertilized chicken eggs (Goto Furanjo, Kakamigahara, Japan) were kept in a humidified incubator at 37˚C. Ovalbumin was removed from 4-day-old embryonated eggs. A small hole was drilled on eggshell and capped, and the eggs were incubated at 37˚C. Following 24 h of incubation, 0, 0.2, 1.0 or 5.0 μM PPI were applied to the center of silicon rings that were placed on each CAM, and the eggs were incubated at 37˚C. Following a 2-day incubation, fat emulsion (Intralipos®; Otsuka Pharmaceutical Co., Ltd.) was injected into the chorioallantois. The blood vessels were photographed using Light Capture II (ATTO Corp.) at a magnification of x5. Angiogenesis was quantified by measuring the total number of blood vessels, the total number of branches of blood vessels seen in each silicon ring and the total length of blood vessels per diameter of the ring. In total, 6-7 eggs were used in each treatment group and the assay was performed more than once to confirm the results.

Tumor xenograft assay. A total of 15 female BALB/cSlc-*nu/nu* mice, aged 6 weeks old were purchased from Japan SLC, Inc. All mice were quarantined for 1 week and housed in plastic

cages (3-4 mice/cage, weighing 16.7±0.15 g) with free access to tap water and a basal diet (MF; Oriental Yeast Co. Ltd.) under controlled conditions of humidity (50±10%), temperature (23±2˚C) and lighting (12 h light/12 h dark cycle; 8:00 a.m. lights on, 8:00 p.m. lights off). Animal experiments were performed with the approval of the Animal Ethics Committee of the Nagoya City University (approval no. H25M-16) and according to the guidelines of the committee. Viable HT29 human colon carcinoma cells ($2.5x10^6$ cells/200 μl DMEM without L-glutamine and phenol red) were subcutaneously injected into the flanks of the mice. After confirming the visible tumor mass, mice were assigned into 2 experimental groups. PPI was dissolved in soybean oil (FUJIFILM Wako Pure Chemical Corporation). The mice in group 1 (n=7, vehicle-control) and group 2 (n=8, treatment) received intraperitoneal (i.p.) injections of the vehicle (soybean oil) and 50 mg/kg PPI, respectively, once per day for 10 days (a total of 4 times) until the end of the experiment. The animals were observed on a daily basis for tumor growth, body weight and symptomatic adverse side-effects. Tumors were measured twice a week. The mean volume per tumor was calculated using the following formula: V (mm^3)=LxWxDxπ/6 where 'V' is the volume, and 'L' is the length, 'W' is the width, and 'D' is the depth of the tumor (22). At 49 days after the inoculation, all animals were sacrificed by decapitation following anesthesia with 3% isoflurane and a complete autopsy was performed. Tumors were carefully removed, fixed with 10% buffered formalin and processed for histopathological examination [hematoxylin (9131-2, Sakura Finetek Japan Co., Ltd.) and eosin (1B-425, Nacalai Tesque, Inc.) (H&E) staining]. Tumors were stained with hematoxylin at room temperature for 2 min and eosin at room temperature for 10 min. Furthermore, necrosis and viable areas (mm^2) in the H&E-stained tumor sections (3 μm in thickness) were measured using an imaging system (Digital Microscope VHX-5000, Keyence Corporation). The percentage necrotic area was calculated, with 100% representing a total area (necrosis plus viable areas) of the tumor.

Immunohistochemical analysis. The assay was performed using a BOND-MAX automated immunohistochemistry system (Leica Biosystems GmbH) as previously described (23). The paraffin-embedded tumor sections (3-μm-thick) were boiled in 10 mM citric acid buffer solution (pH 6.0) at 100˚C for antigen retrieval, and incubated with primary antibodies to p-STAT3 (#9145, 1:50) at room temperature for 1 h, cleaved caspase-3 (#9661, 1:100) at 4˚C overnight, or CD34 (#3569, 1:100) (all from Cell Signaling Technology, Inc.) at room temperature for 30 min. Primary antibody was detected using biotinylated secondary antibody (VECTASTAIN ABC Standard kit, PK-4000, Vector Laboratories, Inc.) and diaminobenzidine (DAB). Incubation was performed at room temperature for 5 min. The sections were counterstained with hematoxylin at room temperature for 30 sec or 5 min. The number of blood vessels was measured in a specific structure consisting of CD34-positive vascular endothelial cells in the viable area of the tumor. In total, >10 fields were examined in each section. The p-STAT3-positive rate (%) was determined by calculating the ratio of the p-STAT3-positive cells/total number of cells counted (Olympus DP70, Olympus 3-CCD COLOR CAMERA CS530 MD, Olympus Corp., Tokyo, Japan). In this assay, >10 fields were examined in each section. p-STAT3-positive cells were determined by setting a consistent threshold for all slides using image J software (National Institutes of Health). In the present study, the apoptotic index was defined by calculating the number of cleaved caspase-3-positive cells per mm^2.

Rat model of colon ACF. This experiment was performed as described in previous studies (4,24). Male F344 rats (n=18, 4 weeks old, weighing 72.3±0.91 g, Japan SLC, Inc.) were used in this experiment. All rats were quarantined for 1 week and maintained as described in a mouse bioassay system in this section. A total of 18 rats were randomly divided into 4 groups. Rats in groups 1-3 were administered a subcutaneous injections of 20 mg/kg azoxymethane (AOM, CAS no. 25843-45-2, purity >95%, FUJIFILM Wako Pure Chemical Corporation) twice a week. At 2 days after the final injection of AOM, rats in group 1 received i.p. injections of soybean oil (FUJIFILM Wako Pure Chemical Corporation) and rats in groups 2 and 3 received i.p. injections of 2 and 10 mg/kg PPI, respectively, once per 10 days (a total of 4 times until the end of the experiment). The rats in group 4 were administered the basal diet alone throughout the experiment and served as an untreated control. Animals were observed on a daily basis for body weight changes and symptomatic adverse side-effects during the experiment. At the week 7, all animals were sacrificed by decapitation following anesthesia with 3% isoflurane and a complete autopsy was performed. Colon tissues were removed, cut longitudinally and fixed with 10% buffered formalin. After fixing, colon tissues (≤1 mm in thickness) were stained with 0.2% methylene blue solution (M9410, Sigma-Aldrich; Merck KGaA) at room temperature for 30 sec. Using a microscope system (Leica Application Suite ver. 4, Leica Biosystems GmbH), the numbers of ACF were counted according to the criteria described by Bird (25). The number of ACF per colon (multiplicity) and the number of crypts per one focus were determined as previously described by the authors (24). These animal experiments were performed with the approval of the Animal Ethics Committee of the Nagoya City University (approval no. H25M-44) and according to the guidelines of the committee.

Statistical analysis. Statistical analysis was performed with EZR (Saitama Medical Center, Jichi Medical University) (26). Comparisons between the vehicle-treated control group and the PPI-treated group in the xenograft model were made using a Student's t-test, Welch's t-test, or Mann-Whitney U test. As regards the data of the luciferase reporter assay, CAM assay and the animal experiments, ANOVA or the Kruskal-Wallis test, as needed were used, and the Bonferroni/Dunn, Steel's-Dwass test, or Tukey's multiple comparison tests were applied to evaluate statistical significance. All results are expressed as the means ± SE. Differences between groups at $P<0.05$ were considered statistically significant.

Results

PPI inhibits the growth of human colon carcinoma cells. As shown by the colony formation assay, PPI induced a marked and dose-dependent inhibition of the growth of the HT29,

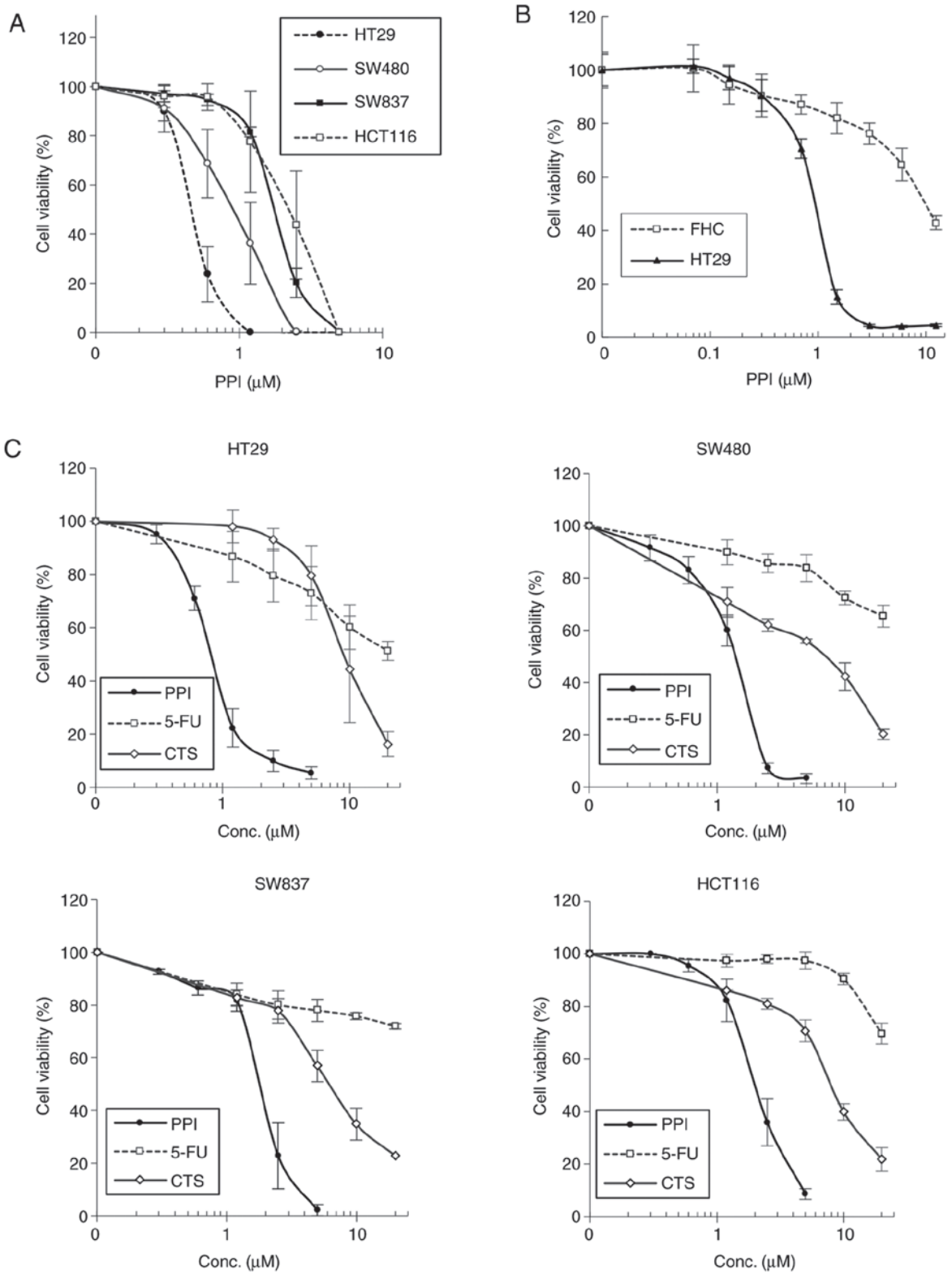

Figure 2. Inhibition of cell growth by PPI in human colon carcinoma cell lines. (A) Colony formation assays. These colon carcinoma cell lines were tested. Exponentially dividing cells were treated with 0.25-5.0 μM PPI for 7 days in DMEM containing 10% FBS, and colonies were then stained and counted. (B) MTT assays. Growth curves of HT29 and FHC cell lines were indicated Cells were treated with 0.07-12.5 μM PPI for 96 h in DMEM containing 10% FBS. (C) MTT assays. Three agents (PPI, 5-FU and CTS) were tested in each cell line (HT29, SW480, SW837 and HCT116). Cells were treated with 0.25-5.0 μM PPI, 1.2-20 μM 5-FU, and 1.2-20 μM CTS for 48 h in DMEM containing 10% FBS. Error bars indicate the standard error (SE) in each panel. For additional details, please see the 'Materials and methods'. PPI, palmitoyl piperidinopiperidine; 5-FU, 5-fluorouracil; CTS, cryptotanshinone.

SW480, SW837 and HCT116 cell lines, with IC_{50} values of approximately 0.5, 1.0, 1.9 and 2.2 μM, respectively (Fig. 2A). To examine the cytotoxic effects of PPI on the FHC human colon normal epithelial cell line, the cells were treated with increasing concentrations (0.07-12.5 μM) of PPI or acetone (≤0.5%, control) for 96 h, and cell growth was then determined

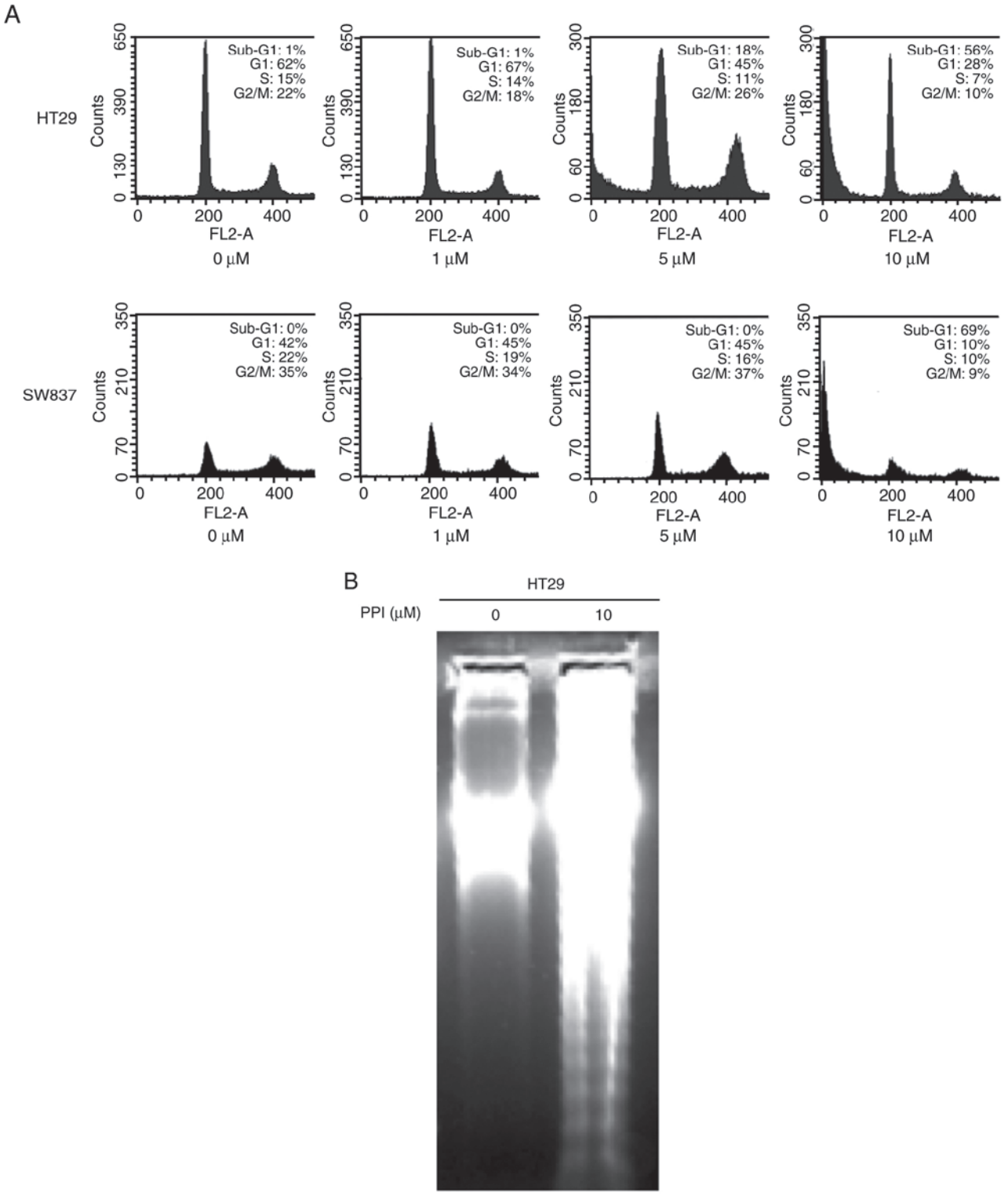

Figure 3. Effects of PPI on cell cycle progression and apoptosis. (A) Representative results of flow cytometric analysis. Exponentially growing HT29 and SW837 cells were treated with 0.1% acetone (control) or 1, 5 and 10 μM PPI in DMEM/10% FBS. Following treatment for 48 h, the cells were analyzed by DNA flow cytometry. (B) Representative results of the detection of DNA fragmentation. HT29 cells were treated with acetone or 10 μM PPI for 48 h in DMEM plus 10% FBS. DNA was extracted and agarose gel electrophoresis was performed as described in the 'Materials and methods'. A 'DNA ladder' representing fragmented DNA (right lane) was observed, when compared to the control (left lane). PPI, palmitoyl piperidinopiperidine.

by MTT assays (Fig. 2B). When the HT29 colon carcinoma cells were treated with 1.5 μM PPI, approximately >90% of the cells died but at the same concentration of PPI, but approximately 80% of the normal colon epithelial cells survived without any significant morphological abnormalities, indicating that this drug selectively kills carcinoma cells at an effective dose level. As shown in Fig. 2C, in the HT29, SW480, SW837 and HCT116 cell lines, PPI induced a marked growth inhibitory effect in a dose-dependent manner, with IC_{50} values of approximately 0.8, 1.4, 2.0 and 2.1 μM, respectively, when the cells were

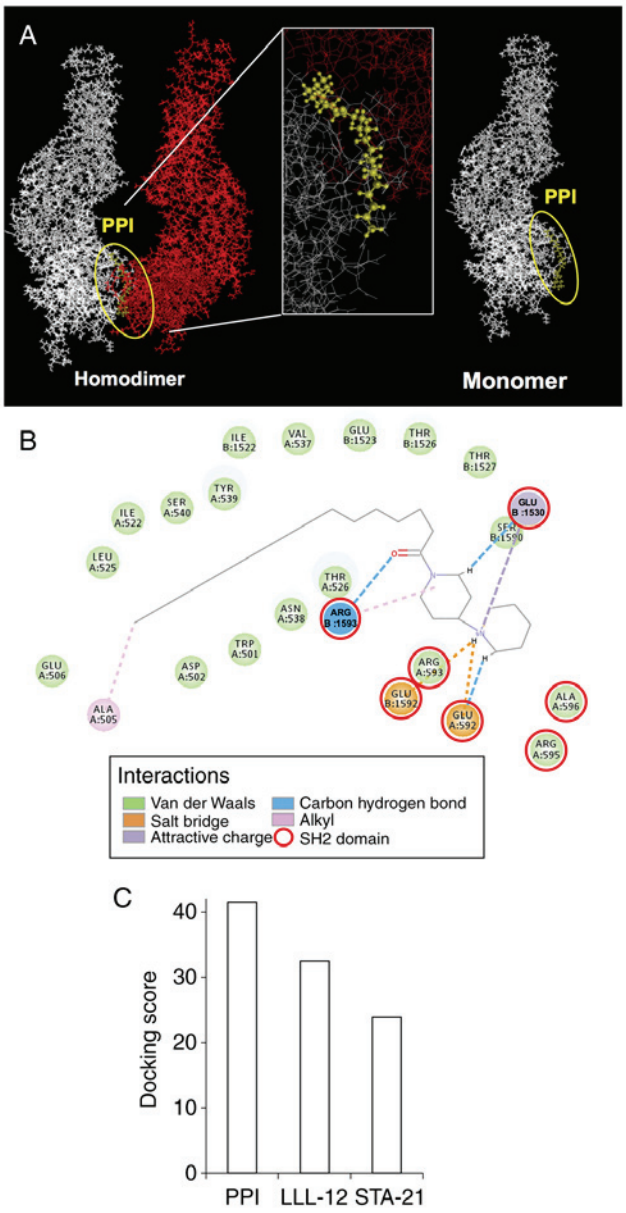

Figure 4. Schematic diagram of modeling of *in silico* molecular docking analysis (virtual screening). (A) Predicted binding model of PPI to the STAT3 SH2 domain. The structure is based on Protein Data Bank entry 3CWG (STAT3). Ball-and-stick models of a homodimer (left panel) and a monomer (right panel) of the STAT3 protein are shown. Each monomer structure is indicated in different color (white and red). The circled region in yellow indicates the chemical structure of PPI. The center panel indicates the predicted binding model of PPI to the STAT3 SH2 domain. (B) Specific interactions formed between the STAT3 SH2 domain and PPI. The binding model was predicted by the CDOCKER protocol. Amino acid residues that form interactions with PPI are shown in the 2D diagram. (C) -CDOCKER_ENERGY obtained from the docking analysis indicates docking score. As a result of this calculation, PPI demonstrated higher docking score than that of the STAT3 SH2-specific inhibitors, LLL-12 (35) and STA-21 (36). PPI, palmitoyl piperidinopiperidine; STAT3, signal transducer and activator of transcription 3.

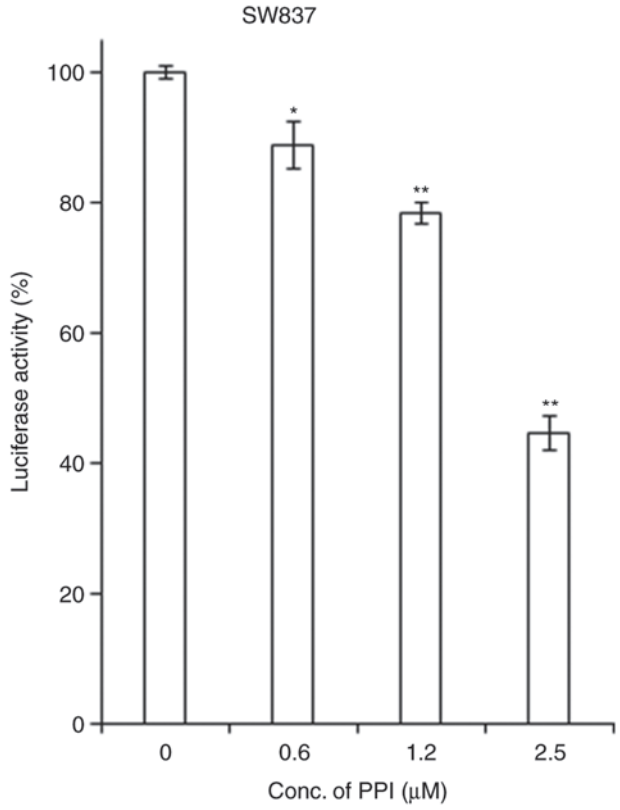

Figure 5. Effect of PPI on the transcriptional activity of the STAT3 reporter vector. The STAT3-luciferase reporter (1.0 μg) was transfected into SW837 cells, and the transfected cells were treated for 24 h with 0.5% acetone (control) or 0.6, 1.2 or 2.5 μM PPI in DMEM/10% FBS. Extracts were then examined for luciferase activity. In this assay, a CMV promoter β-gal plasmid was co-transfected with the STAT3 reporter, and β-gal activity was measured to normalize the data for transfection efficiency. All assays were done in triplicate. Error bars indicate the SE in each panel (*P<0.05, **P<0.01 compared to untreated cells). PPI, palmitoyl piperidinopiperidine; STAT3, signal transducer and activator of transcription 3.

treated with increasing concentrations (0.25-5.0 μM) of PPI or 0.1% acetone (control) for 48 h, and cell growth was then measured by MTT assays. As observed in the growth curves, the IC_{50} value of PPI in each cell line was markedly lower than that of 5-FU or CTS, indicating that PPI exerted more potent inhibitory effects in this assay system (Fig. 2C).

PPI induces an increase in the number of cells in the G1 phase of the cell cycle, and induces sub-G1 fractions of cells at a higher concentration level. Cell cycle analysis was performed to examine whether the PPI-treated cells arrest in a specific phase of the cell cycle and whether PPI induces the sub-G1 fractionation of cells. Flow cytometric analysis indicated that when the HT29 and SW837 cells were treated with 1 μM PPI for 48 h, the percentage of cells in the G1 phase increased by 5 and 3%, respectively, and this was associated with a concomitant decrease in the number of cells in the S and G_2-M phase of the cell cycle (Fig. 3A). Only when the HT29 and SW837 cells were treated with higher concentrations (5 or 10 μM) of PPI for 48 h, they began to detach from the culture dish and displayed evidence of apoptosis by an increase in the sub-G1 population of cells (Fig. 3A). Additional experiments detecting DNA fragmentation were performed with the HT29 cells, as described below.

PPI induces the fragmentation of DNA in HT29 cells. The appearance of a 'DNA ladder' was observed in a sample treated with 10 μM PPI on agarose gel electrophoresis (Fig. 3B), demonstrating the induction of apoptosis under the current experimental condition.

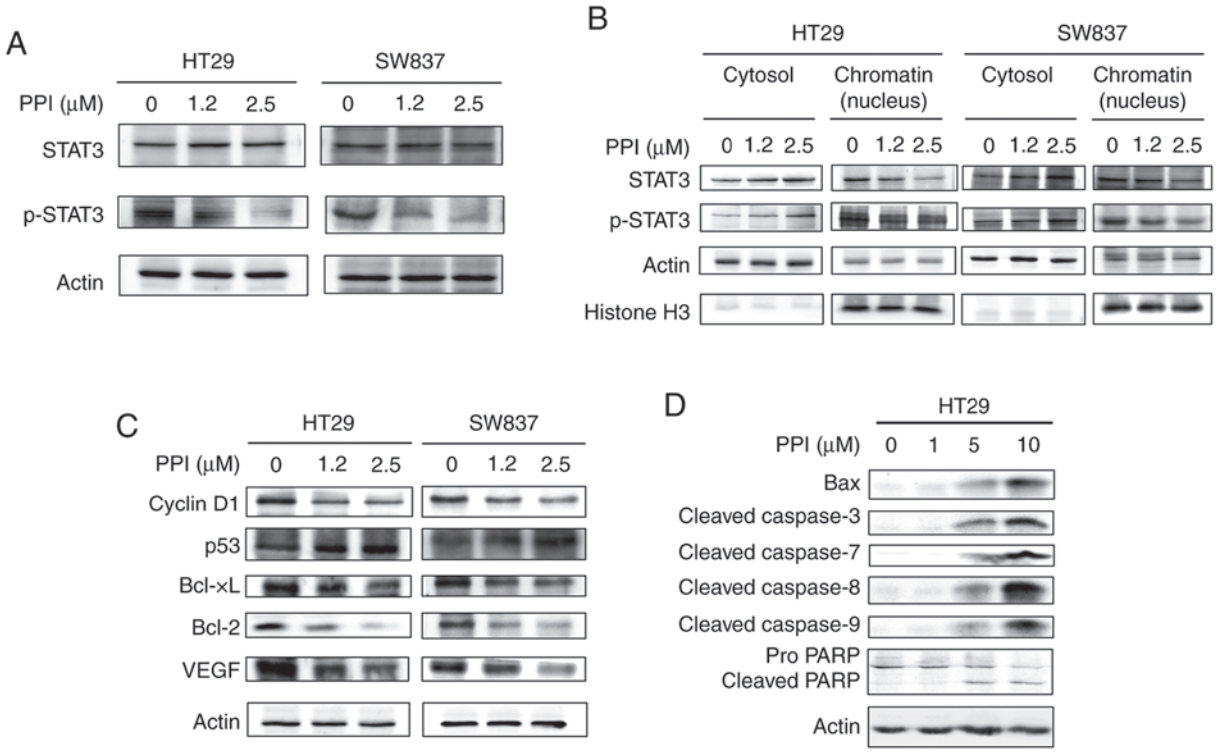

Figure 6. Effects of treatment of the HT29 and SW837 cells with PPI on the expression levels of p-STAT3/STAT3, STAT3-driven proteins and apoptosis-related proteins. (A-C) Cells were treated with 0.5% acetone or the indicated concentrations (1.2 or 2.5 μM) of PPI for 24 h in DMEM/10% FBS. Cell extracts were then examined by western blot analysis for the indicated proteins, using the respective antibodies, as described in the 'Materials and methods'. (D) HT29 cells were treated with 0.5% acetone or the indicated concentrations (1.0, 5.0 or 10 μM) of PPI for 48 h in DMEM/10% FBS, and extracts were examined by western blot analysis. Representative results are shown. PPI, palmitoyl piperidinopiperidine; STAT3, signal transducer and activator of transcription 3.

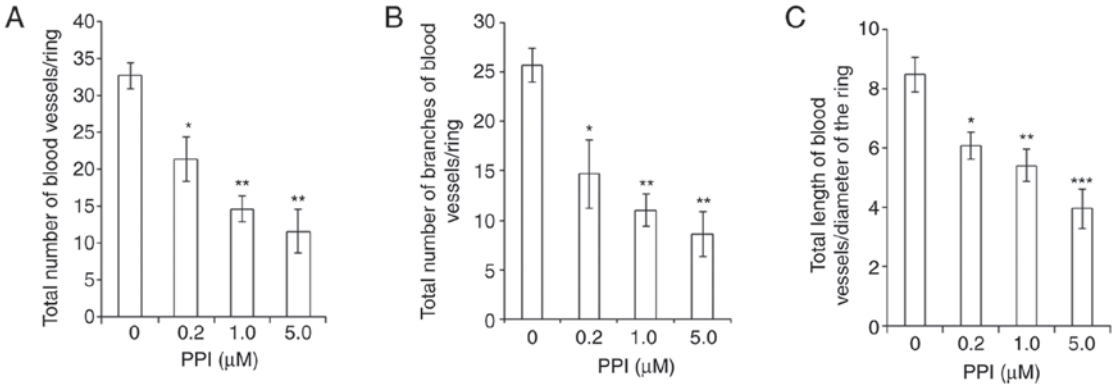

Figure 7. Effect of PPI on angiogenesis in chick chorioallantoic membrane (CAM). (A-C) CAM was exposed to 0.2, 1.0, and 5.0 μM PPI for 48 h and the (A) total number of blood vessels, (B) total number of branches of blood vessels observed in each silicon ring, and (C) the total length of blood vessels per diameter of the ring were measured by an image analyzer. There was a marked and dose-dependent decrease in the total number of blood vessels/ring ($P<0.001$), total number of branches of blood vessels/ring ($P<0.001$) and total length of blood vessels/diameter of the ring ($P<0.001$). Error bars indicate the SE in each panel. $^{*}P<0.05$, $^{**}P<0.01$ and $^{***}P<0.001$ compared to untreated cells. PPI, palmitoyl piperidinopiperidine.

Binding mode of PPI. Previous research has demonstrated that the STAT3 transcription factor plays an important role in the development and progression of a wide range of cancers, including colon cancer, by regulating cell proliferation, cell cycle progression, cell survival, angiogenesis, immune evasion and epithelial-mesenchymal transition (27). In fact, constitutive activation of STAT3 is frequently seen in human cancers including colorectal cancer (28). The present study also found that PPI inhibited the growth of human colon carcinoma cell lines as described above. Furthermore, a critical step in STAT3 activation is the dimerization between two STAT3 monomers, and this step is dependent on the reciprocal binding of the SH2 domain of one STAT3 monomer to the other monomer (29). Thus, to understand the interaction between PPI and the protein STAT3, PPI was docked in the active site of STAT3 (PDB code: 3CWG). As shown in Fig. 4A, PPI exhibited shape complementarity with the binding pocket of the SH2 domain of STAT3. The carbon, oxygen, nitrogen, or hydrogen atoms of PPI formed interactions, such as alkyl, salt bridge, carbon hydrogen bond, van der Waals or attractive charge, and came

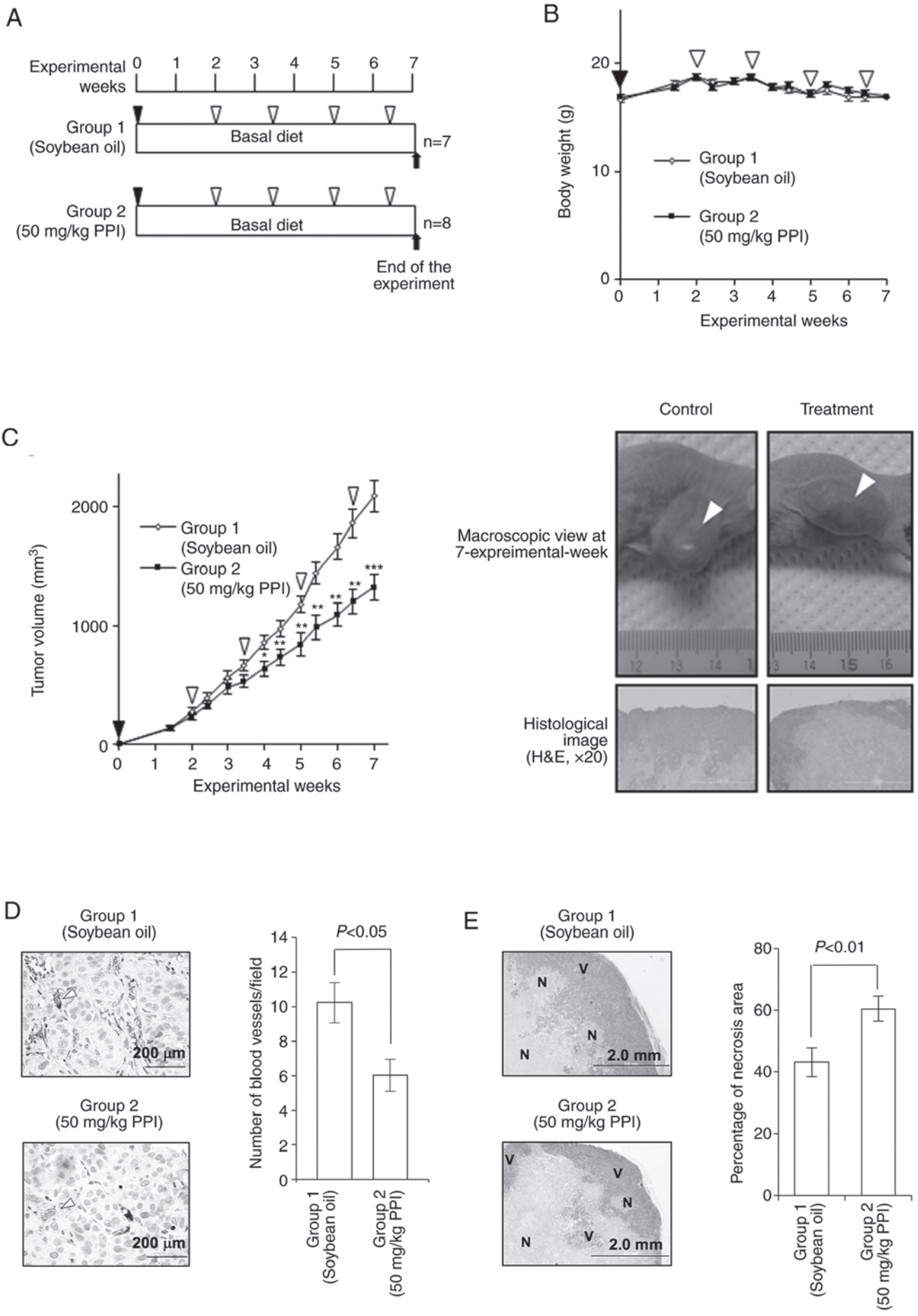

Figure 8. Continued.

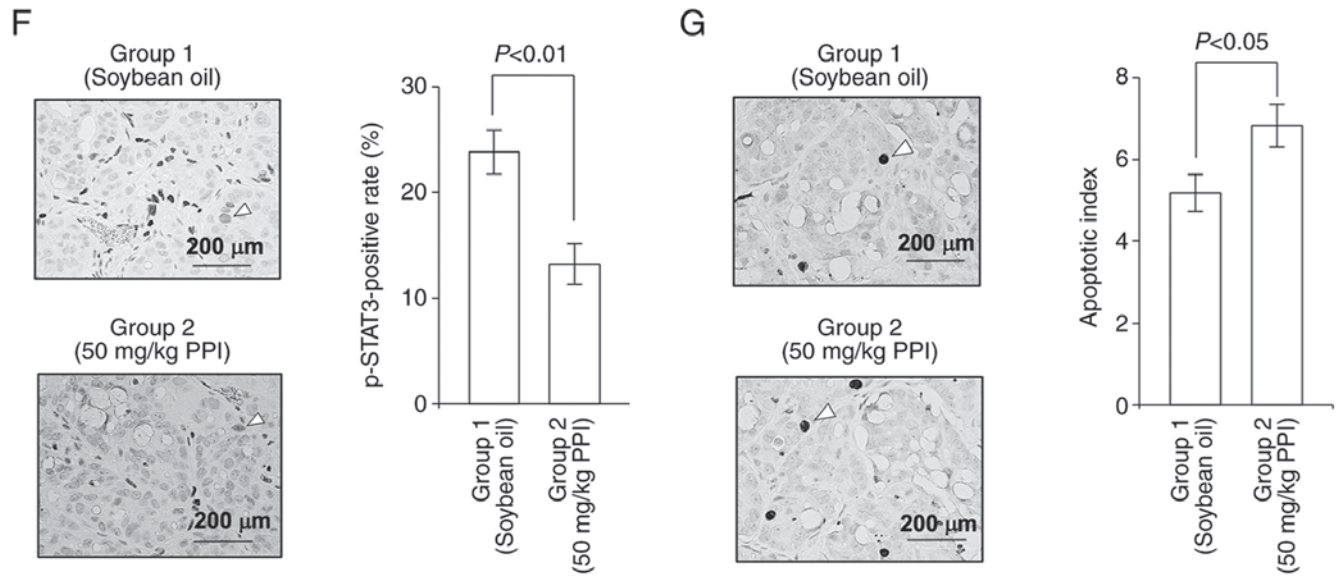

Figure 8. Effects of PPI in a mouse xenograft model. (A) Experimental protocol. After inoculation of viable HT29 human colon carcinoma cells into the flanks of mice, the animals were administered intraperitoneal injections of soybean oil (control) or 50 mg/kg PPI once per 10 days (a total of 4 times) until the end of the experiment. (B) Time-course record of body weight during the experiment. Treatment of mice with PPI did not cause a significant body weight loss during experiment. Black arrowheads indicate the inoculation of HT29 cells; white arrowheads indicate intraperitoneal injections of soybean oil (group 1) or 50 mg/kg PPI (group 2). (C) Tumor volume during the experiment (left panel). A marked decrease in tumor volume was observed after 4 experimental weeks (*P<0.05, **P<0.01 and ***P<0.001). Representative images of animals with tumors are also shown (right panel). Arrowheads indicate the tumor mass in the right flank of the mice, and histological images are also shown. The tumor of the control measured 17.2 mm in length, 16.4 mm in width and 12.2 mm in depth. The tumor of the treatment group measured 17.8 mm in length, 12.9 mm in width and 9.4 mm in depth. (D) Representative images of CD34 immunohistochemical staining of the tumor. Vehicle control (soybean oil, left upper panel), PPI treatment (left lower panel), and the number of CD34-positive blood vessels (right panel) are shown. (E) Vehicle control (soybean oil, left upper panel), PPI treatment (left lower panel) and percentage of necrosis area are shown. This value was calculated, with 100% representing a total area (necrosis plus viable areas) of the tumor. 'N' and 'V' indicate necrosis and viable areas, respectively. (F and G) p-STAT3-positive rate (%) and apoptotic index are shown, respectively. Representative images of (F) p-STAT3 and (G) cleaved caspase-3 immunohistochemical staining of the tumor are demonstrated in vehicle-control (soybean oil, left upper panel), PPI treatment (left lower panel). Arrowheads indicate positively stained cells with each antibody. Error bars indicate the SE in each panel. PPI, palmitoyl piperidinopiperidine; STAT3, signal transducer and activator of transcription 3.

into close contact with the amino acid residues, Trp, Asp, Ala, Glu, Ile, Leu, Thr, Val, Asn, Tyr, Ser, or Arg (Fig. 4B). The binding affinity was evaluated by the -CDOCKER_ENERGY (kcal/mol) obtained from the docking analysis of a compound of interest. As a result of this calculation, PPI exhibited a higher -CDOCKER_ENERGY than that of the conventional specific inhibitors, LLL-12 and STA-21, of the SH2 domain of STAT3 (Fig. 4C).

PPI inhibits the transcriptional activity of STAT3. Based on the above-mentioned finding that PPI can bind to SH2 domain of STAT3 in a molecular docking analysis, the present study then examined the effects of PPI on the transcriptional activity of the STAT3 in transient transfection luciferase reporter assays using a STAT3 reporter. It was found that treatment with PPI led to a dose-dependent decrease in the activity of the STAT3 reporter in SW837 cells (Fig. 5).

Effects of PPI on the expression levels of STAT3 and p-STAT3 in whole lysate samples and cytosol/chromatin fraction samples. As it was found that PPI inhibited the transcriptional activity of STAT3 in a dose-dependent manner, western blot analysis was performed to determine whether treatment of the HT29 and SW837 cells with PPI alters the cytosolic or nuclear levels of the STAT3 and phosphorylated form of STAT3 (p-STAT3) in 3 different fractions of cell lysates. In the whole cell lysate samples, it was found that treatment of the HT29 and SW837 cells with 1.2 or 2.5 μM PPI led to a marked decrease in the expression levels of p-STAT3, but not those of STAT3 in these cells (Fig. 6A). In the HT29 and SW837 cell lines, treatment of the cells with 1.2 or 2.5 μM PPI led to a decrease in the expression levels of both STAT3 and p-STAT3 in the chromatin fraction (Fig. 6B). In the HT29 and SW837 cells, treatment of these cells with 1.2 or 2.5 μM PPI led to an increase in the expression levels of both STAT3 and p-STAT3 in the cytosolic fraction (Fig. 6B).

Effects of PPI on the expression levels of cell cycle-related and STAT3-driven molecules. Due to the finding that PPI induced G1 arrest in the cell cycle (Fig. 3A) and that PPI inhibited the expression levels of p-STAT3 (Fig. 6A), the present study wished to determine whether treatment of the HT29 and SW837 cells with 1.2 or 2.5 μM PPI alters the cellular levels of the G1 cell cycle control protein cyclin D1, the cell cycle inhibitor protein p53 and STAT3-driven molecules. It was found that treatment with PPI led to an increase, in p53 and a decrease in cyclin D1, Bcl-xL, Bcl-2 and VEGF expression (Fig. 6C). These changes occurred in a dose-dependent manner.

Effects of PPI on the levels of expression of apoptosis-related molecules. From the above-mentioned findings, it could be inferred that PPI induced the apoptosis of the HT29 cell line. Thus, it was of interest to determine whether PPI affects the cellular levels of apoptosis-related molecules. HT29 cells

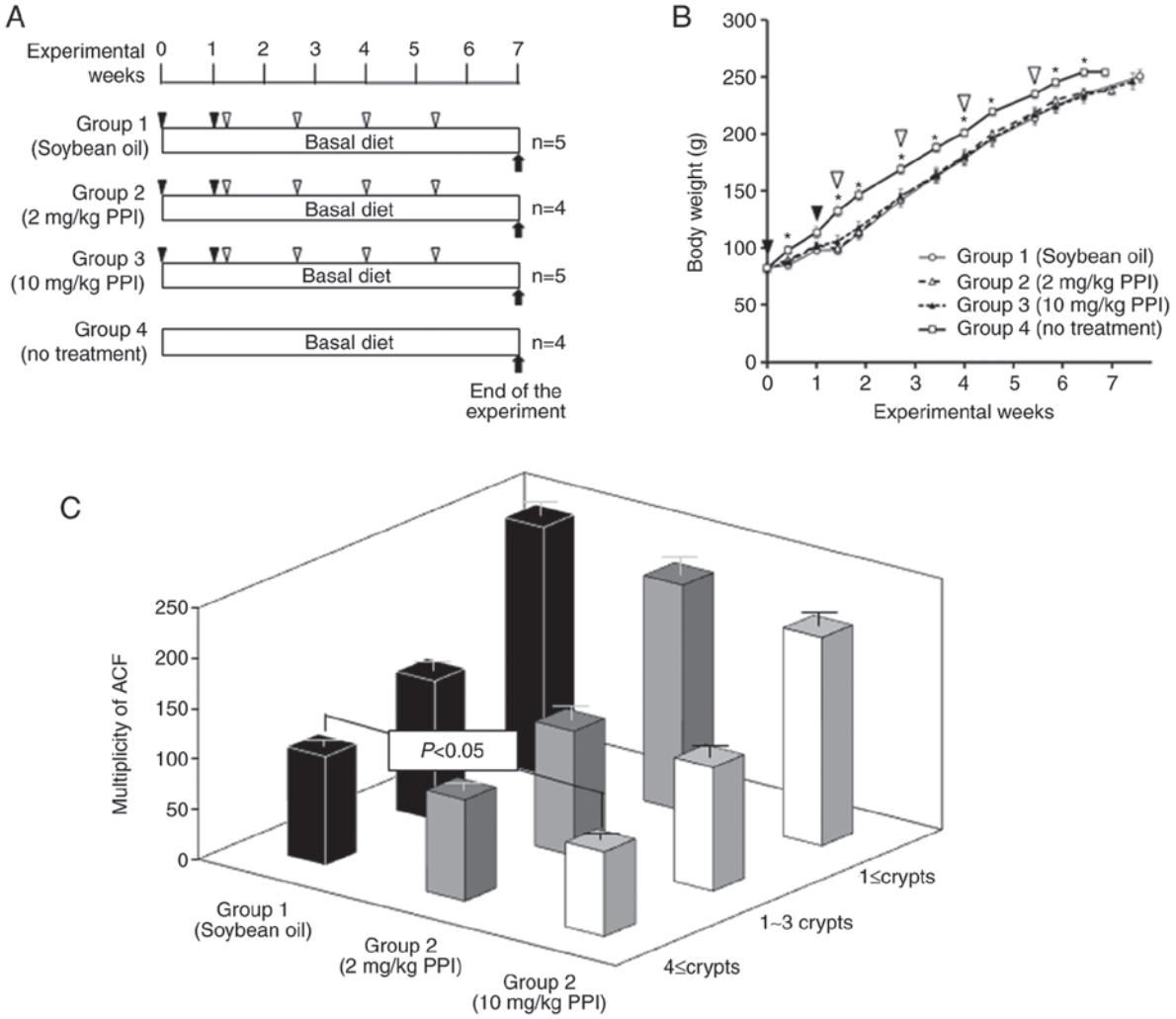

Figure 9. Effects of PPI on tumor promotion in a rat colonic aberrant crypt foci (ACF) model. (A) Experimental protocol. F344 rats received subcutaneous injections of a carcinogen AOM and then treated with soybean oil or PPI. (B) Time-course record of body weight during the experiment. There was no significant decrease in body weight between PPI-treated groups (groups 2 and 3) and vehicle-treated control group (group 1) during experiment. However, there was a significant decrease in body weight of the PPI-treated groups (groups 1-3) when compared to that of the no treatment group (group 4) due to the effect of the administration of the carcinogen, azoxymethane (AOM; *P<0.05). Black arrowheads indicate subcutaneous injections of AOM; white arrowheads indicate intraperitoneal injections of soybean oil (group 1), 2 mg/kg PPI (group 2), or 10 mg/kg PPI (group 3). (C) Number of ACF per colon (multiplicity) and the number of crypts per one focus in each group are shown. PPI significantly inhibited the multiplicity of larger ACF consisting of ≥4 aberrant crypts. Error bars indicate the SE in each panel. For additional details, please see the 'Materials and methods'. PPI, palmitoyl piperidinopiperidine.

were treated with 0.2% acetone (control) or with increasing concentrations (1, 5 and 10 μM) of PPI for 48 h. PPI induced a marked and dose-dependent increase in the expression levels of Bax, cleaved caspase-3, cleaved caspase-7, cleaved caspase-8, cleaved caspase-9 and cleaved PARP (Fig. 6D). PPI also induced a concomitant decrease in the expression levels of pro PARP when the carcinoma cells were treated with 5 or 10 μM (Fig. 6D).

Inhibitory effects of PPI on the angiogenesis of the CAM. From the above-presented results of western blot analyses, it was found that PPI inhibited the expression level of VEGF (Fig. 6C), a key mediator of angiogenesis. Thus, the anti-angiogenic effect of PPI was also examined *in vivo* using CAM assays. A marked and dose-dependent inhibition of the angiogenesis of the CAM was observed (Fig. 7). There was a marked and dose-dependent decrease in the total number of blood vessels/ring (P<0.001; Fig. 7A), the total number of branches of blood vessels/ring (P<0.001; Fig. 7B) and the total length of blood vessels/diameter of the ring (P<0.001; Fig. 7C).

Growth inhibitory and anti-angiogenic effects of PPI in a xenograft model. As the above-described *in vitro* assays provided evidence that PPI inhibits the *in vitro* growth of human colon carcinoma cells (Fig. 2) and the angiogenesis of CAM (Fig. 7), it was of interest to determine whether PPI also exerts potent inhibitory effects on tumor growth and angiogenesis *in vivo*. All the BALB/cSlc-*nu/nu* mice in the present study survived (the experimental protocol is illustrated in Fig. 8A). Treatment of the mice with PPI did not cause significant body weight loss during the experiment (Fig. 8B). Body weight (g) at the end of each treatment was 17.9±0.40 (group 1) and 18.1±0.29 (group 2). After 4 experimental weeks, treatment of the mice with 50 mg/kg PPI (group 2) resulted in a significant decrease in tumor volume when compared to the control vehicle-treated

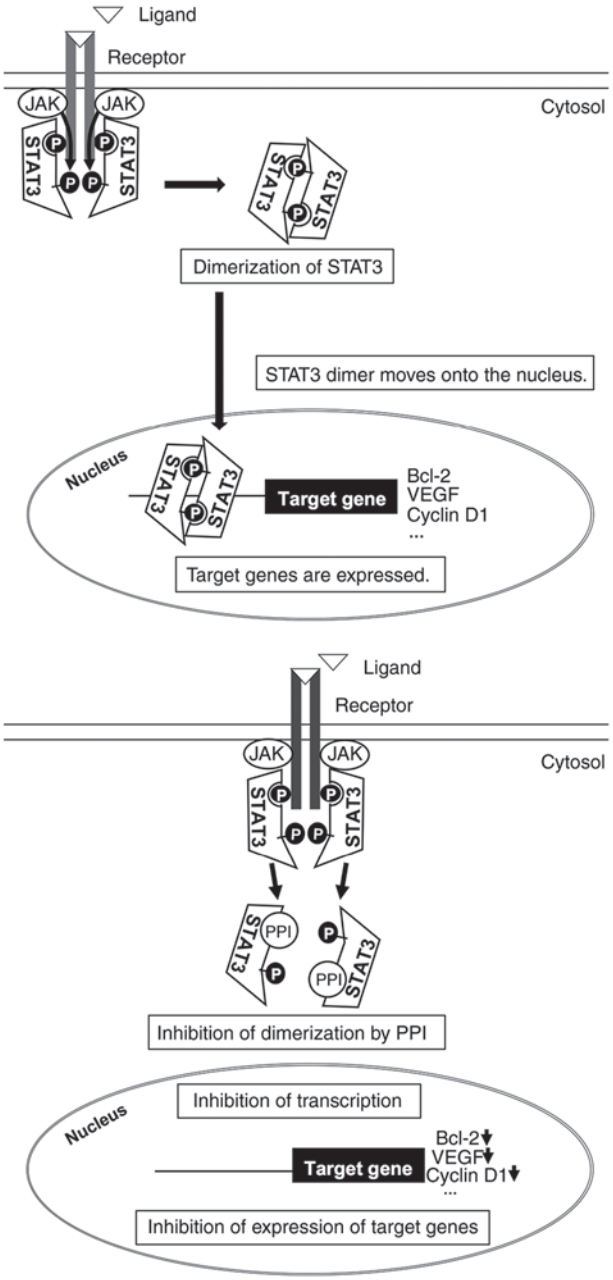

Figure 10. Hypothetical anticancer mechanism of action of PPI. STAT3 is activated by Janus Kinase (JAK)-mediated phosphorylation at tyrosine residue 705 (Tyr-705), which leads to dimerization, nucleus translocation, recognition of STAT3 specific DNA binding site, and activation of target gene transcription including Bcl-2, VEGF and cyclinD1 (upper panel). The dimerization of STAT3 depends on the reciprocal binding of the SH2 domain of one monomer to the specific segment of the other STAT3 monomer. PPI binds to SH2 domain of STAT3 and blocks its dimerization. STAT3 is then inactivated. The drug PPI we invented is able to exert anticancer activity at lead in port by inhibiting transcriptional activity of STAT3. This action of PPI leads to the suppression of function molecules that are related to apoptosis, angiogenesis and cell cycle progression (lower panel). PPI, palmitoyl piperidinopiperidine; STAT3, signal transducer and activator of transcription 3.

mice (group 1) (P<0.001; Fig. 8C). Treatment of the mice with 50 mg/kg PPI resulted in a significant decrease in the number of blood vessels compared to the controls (Fig. 8D). Collectively, these results demonstrate that PPI exerts a potent inhibitory effect on angiogenesis *in vivo*.

PPI induces an increase in the necrotic area in implanted tumors. As it was found that there was a significant decrease in tumor volume in the PPI-treated group, the present study then investigated its effects on the induction of apoptosis by determining the area in which cells underwent apoptosis with a microscope imaging system. There was a significant increase in the necrotic area of the PPI-treated tumors compared to that of the vehicle-treated tumors (P<0.01; Fig. 8E).

Effects of PPI on the immunohistochemical expression levels of p-STAT3 and apoptotic index in the tumor xenograft model. In view of the above-mentioned findings that PPI induced apoptosis, as shown by flow cytometric analysis and DNA fragmentation assay, the present study then examined the mechanisms through which PPI plays a role in controlling the apoptotic process in the tumor. For this purpose, the effects of PPI were assessed by conducting immunohistochemical analysis using p-STAT3 and cleaved caspase-3 antibodies. Treatment of the mice with PPI led to a significant decrease in the p-STAT3 positive rate of the tumor compared to the control (Fig. 8F) and also led to a significant increase in the apoptotic index compared to the control (Fig. 8G).

Inhibition of the formation of ACF by PPI. To examine whether PPI exerts inhibitory effects in the post-initiation phase of AOM-induced colon carcinogenesis, the well-established and short-term protocol of the rat ACF model system was used (4,24). All rats in the present study survived (the experimental protocol is illustrated in Fig. 9A) and no significant body weight loss was observed between the PPI-treated groups (groups 2 and 3) and the vehicle-treated control group (group 1) during the experiment (Fig. 9B). However, there was a significant decrease in body weight of the PPI-treated groups (groups 1-3) when compared to that of the no treatment group (group 4) due to the effects of the administration of the carcinogen, AOM (Fig. 9B). Body weight (g) at the start of the experiment was 83.0±1.52 (group 1), 84.3±2.53 (group 2), 82.2±2.27 (group 3) and 82.5±2.22 (group 4). Body weight (g) at week 7 was 250.4±5.46 (group 1), 238.0±3.49 (group 2), 246.2±7.14 (group 3) and 254.0±3.08 (group 4). ACF were mainly found in the middle portion of the colon. PPI significantly inhibited the multiplicity of larger ACF consisting of ≥4 aberrant crypts (Fig. 9C). There was a dose-dependent decrease observed in the multiplicity of ACF, although this finding was not statistically significant. These findings indicate that the inhibitory effect on tumor promotion was at least in part via the formation of larger ACF in a carcinogen-induced rat ACF model system.

Discussion

The fact that natural products have been traditionally used worldwide in the prevention and/or treatment of several chronic diseases among various ethnic societies was the inspiration for the present study. It was hypothesized that it would be possible to develop a novel anticancer drug derived from 10-HDA as an initial lead compound by creating a structure-based pharmacophore model as it was found that 10-HDA inhibited the growth of human colon carcinoma cells (Fig. S1) (16). After synthesizing >100 derivatives of

10-HDA (Fig. 1A) and optimizing their structures by quantitative structure-activity relationship (QSAR), the present study eventually obtained one candidate compound, named PPI (Fig. 1B). Several polyamine derivatives resembling PPI in structure were demonstrated in a previous study; however, none of these exhibited potent growth inhibitory activity against leukemia P-388 or human epidermoid carcinoma of the nasopharynx KB cell lines (30). When carcinoma cells were treated with the effective concentration level of PPI, approximately >90% of carcinoma cells died, but at the same concentration, >80% of normal colon epithelial cells survived (Fig. 2B), indicating that this drug selectively kills carcinoma cells under appropriate experimental conditions.

The present study focused on the transcription factor, STAT3, that is highly expressed in colon carcinoma cells or tissues (28) and can drive carcinogenesis- or angiogenesis-related genes (31). STAT3 is activated by phosphorylation at tyrosine residue 705 (Tyr-705), which leads to the dimerization, nucleus translocation, recognition of STAT3 specific DNA binding site (32), and the activation of target gene transcription, including Bcl-2, VEGF and cyclinD1 (31). The dimerization of STAT3 is dependent on the reciprocal binding of the SH2 domain of one monomer to the Pro-pTyr-Leu-Lys-Thr-Lys segment of the other STAT3 monomer (33). *In silico* docking simulation in the present study exhibited that PPI can bind to SH2 domain of STAT3, suggesting that this drug blocks dimerization of STAT3, thereby inactivating its function.

The present study then focused on the mechanisms through which PPI kills human colon carcinoma cells. It was found that PPI inhibits the transcriptional activity of STAT3 and decreases the expression level of the phosphorylated form of STAT3 (p-STAT3). PPI also led to a decrease in the expression level of STAT3 and p-STAT3 in the chromatin fraction (Fig. 6B), suggesting the inhibition of the translocation of these molecules. However, further investigations are necessary to draw firm conclusions on this aspect. Treatment with PPI led to an increase in p53, and a decrease in cyclin D1, Bcl-2, and Bcl-xL expression. Furthermore, there was a marked increase in the levels of expression of Bax, cleaved caspase-3, cleaved caspase-7, cleaved caspase-8, cleaved caspase-9 and cleaved PARP, with a concomitant decrease in the levels of pro PARP. Together with the findings of flow cytometric analysis, PPI induced the dose-dependent inhibition of carcinoma cell growth, and this anti-proliferative effect appears to be due to its ability to induce, at least in part, G1-phase arrest and apoptotic cell death. There are two different pathways that lead to apoptosis: The mitochondrial and death receptor pathways (34). Both pathways utilize caspase to induce apoptosis. In the present study, it was found that PPI induced changes in the protein expression levels of caspases and Bcl-2 family proteins (Fig. 6C and D), indicating at least in part, the involvement of these molecules in apoptosis. In addition, the finding that p53-mutant cell lines HT29 and SW837 are sensitive to the treatment of PPI warrants further investigation. In the present study, STAT3 specific inhibitors (LLL-12 and STA-2) were used (Fig. 4). It has been reported that the IC_{50} values of LLL-12 are 0.16-3.09 μM in several human tumor cell lines (35). In a previous study, treatment of the MDA-MB-468 cells with 20 or 30 μM STA-21 led to a potent inhibitory effect on the growth and survival of these cells (36). In the present study, the IC_{50} values of PPI were 0.5-2.2 μM, suggesting that PPI exerts more potent growth inhibitory effects than LLL-12 or STA-21 in several cell lines tested (35,36).

By performing CAM assay, the present study examined whether this drug inhibits angiogenesis. It was found that PPI inhibited the total number (maximum effect, 65%), length (maximum effect, 53%) and the number of branch of blood vessels (maximum effect, 67%) in CAM, in a dose-dependent manner. In chick CAM, it has been demonstrated that VEGF plays an important role in angiogenesis (37) and that the anti-angiogenic effect may be associated with the expression levels of VEGF (37). In addition, the present study found that treatment of human colon carcinoma cells with PPI led to a marked decrease in the expression level of VEGF. Collectively, the transcriptional inhibition of STAT3 by PPI may be one possible mechanism, where the functional performance of molecules related to apoptosis, angiogenesis and cell cycle progression are affected, and eventually contribute to growth inhibition (Fig. 10). Further studies are in progress to examine the range of anticancer activity of PPI in a spectrum of the current four human colon cancer cell lines.

In a mouse xenograft model, at the end of the experiment, an approximately 40% inhibition in the size of the tumor was observed. PPI induced a significant decrease in the p-STAT3 positive rate by 40%. Furthermore, it was found that the apoptotic index in the tumor tissue increased and the number of CD34-positive blood vessels decreased, indicating the growth inhibition, the induction of apoptosis and the inhibition of angiogenesis *in vivo*. Finally, a rat ACF model system was used to evaluate inhibitory effect of PPI in the post-initiation phase of AOM-induced colon carcinogenesis. ACF are cryptic lesions distinguished by their increased size and thicker epithelial lining (24). Furthermore, ACF have only been observed in the colon of carcinogen-treated mice and rats and recognized as preneoplastic lesions (24). In the present study, F344 rats received subcutaneous injections of the carcinogen, AOM, and were then treated with the vehicle soybean oil or PPI. By counting the number of precancerous lesions, ACF, and comparing it between control and treatment groups, the preventive effects of PPI on the post-initiation phase of AOM-induced colon carcinogenesis were determined. A study of longer duration may be of use to evaluate the inhibitory effect on colon carcinogenesis and toxicity or the adverse side-effects of PPI in clinical trials. In the present study, PPI induced a significant decrease in the multiplicity (no. of ACF per colon) of larger ACF consisting of ≥4 aberrant crypts, presumably demonstrating the inhibitory effect on tumor promotion at least in part via a formation of larger ACF in a carcinogen-induced rat ACF model system. ACF range in size and have from 1 to 412 aberrant crypts per focus (38-41). The size in the topographic view and histologically dysplastic feature of ACF are critical factors when ACF are distinguished as preneoplastic lesions (23). In histological slides, large ACF exhibit dysplasia and can thus be termed as microadenoma (24). Therefore, PPI may target more malignant population of affected cells, although this aspect warrants further investigation.

Acknowledgements

The authors would like to thank Dr Sachi Sri Kantha (Gifu University, Gifu Pharmaceutical University) for providing critical discussions and comments; Mr. Kenta Moriwaki, Mr. Yasuaki Isoda, Mr. Keigo Sato (Graduate School of Medical Sciences and Medical School, Nagoya City University) and Dr Munehiro Yamada (NOF Corp., Chemicals Research Laboratory, Amagasaki, Japan) for their excellent technical assistance; and Dr Takamitsu Morioka, Dr Shizuko Kakinuma and Dr Yoshiya Shimada for the use of the analyzing device (Department of Radiation Effects Research, National Institute of Radiological Sciences, National Institutes for Quantum and Radiological Science and Technology, Chiba, Japan). The authors also wish to acknowledge the assistance of the Research Equipment Sharing Center at the Nagoya City University.

Funding

The present study was supported in part by grants from the Ministry of Education, Culture, Sports, Science and Technology of Japan (grant nos. 22501050, 25430154 and 17K07223 to MS).

Availability of data and materials

All data generated or analyzed during the current study are included in the current article.

Authors' contributions

SA, MI and MS designed the study. SA, EY, KF, HM, MI and MS performed the experiments and acquired the data. SA, EY, KF, HM, MI and MS analyzed and interpreted the data. SA, KF, MI and MS wrote, reviewed and/or revised the manuscript. MI and MS contributed to the material management. MS supervised the study. All the authors are fully aware of the contents of this paper, and all authors read and approved the final manuscript.

Ethics approval and consent to participate

All animal experiments were performed with the approval of the Animal Ethics Committee of the Nagoya City University (approval nos. H25M-16 and H25M-44) and according to the guidelines of the committee.

Patient consent for publication

Not applicable.

Competing interests

The authors declare that they have no competing interests.

References

1. Surh YJ: Cancer chemoprevention with dietary phytochemicals. Nat Rev Cancer 3: 768-780, 2003.
2. Lee KW, Bode AM and Dong Z: Molecular targets of phytochemicals for cancer prevention. Nat Rev Cancer 11: 211-218, 2011.
3. Ishihara M, Naoi K, Hashita M, Itoh Y and Suzui M: Growth inhibitory activity of ethanol extracts of Chinese and Brazilian propolis in four human colon carcinoma cell lines. Oncol Rep 22: 349-354, 2009.
4. Morioka T, Suzui M, Nabandith V, Inamine M, Aniya Y, Nakayama T, Ichiba T, Mori H and Yoshimi N: The modifying effect of *Peucedanum japonicum*, a herb in the Ryukyu Islands, on azoxymethane-induced colon preneoplastic lesions in male F344 rats. Cancer Lett 205: 133-141, 2004.
5. Morioka T, Suzui M, Nabandith V, Inamine M, Aniya Y, Nakayama T, Ichiba T and Yoshimi N: Modifying effects of *Terminalia catappa* on azoxymethane-induced colon carcinogenesis in male F344 rats. Eur J Cancer Prev 14: 101-105, 2005.
6. Blum MS, Novak AF and Taber S III: 10-Hydroxy-delta 2-decenoic acid, an antibiotic found in royal jelly. Science 130: 452-453, 1959.
7. Lerkcer G, Capella P, Conte LS, Ruini F and Giordani G: Components of royal Jelly: I. Identification of the organic acids. Lipids 16: 912-919, 1981.
8. Sugiyama T, Takahashi K and Mori H: Royal jelly acid, 10-hydroxy-trans-2-decenoic acid, as a modulator of the innate immune responses. Endocr Metab Immune Disord Drug Targets 12: 368-376, 2012.
9. Li X, Huang C and Xue Y: Contribution of lipids in honeybee (*Apis mellifera*) royal jelly to health. J Med Food 16: 96-102, 2013.
10. Chen YF, Wang K, Zhang YZ, Zheng YF and Hu FL: *In vitro* anti-inflammatory effects of three fatty acids from royal jelly. Mediators Inflamm 2016: 3583684, 2016.
11. Yatsunami K and Echigo T: Antibacterial action of Royal jelly. Bull Fac Agr Tamagawa Univ 25: 13-22, 1985.
12. Alreshoodi FM and Sultanbawa Y: Antimicrobial activity of royal jelly. Anti-Infective Agents 13: 50-59, 2015.
13. Sediva M, Laho M, Kohutova L, Mojzisova A, Majtan J and Klaudiny J: 10-HDA, A major fatty acid of Royal jelly, exhibits pH dependent growth-inhibitory activity against different strains of *Paenibacillus larvae*. Molecules 23: 3236, 2018.
14. Townsend GF, Morgan JF, Tolnai S, Hazlett B, Morton HJ and Shuel RW: Studies on the *in vitro* antitumor activity of fatty acids. I. 10-Hydroxy-2-decenoic acid from royal jelly. Cancer Res 20: 503-510, 1960.
15. Yang YC, Chou WM, Widowati DA, Lin IP and Peng CC: 10-hydroxy-2-decenoic acid of royal jelly exhibits bactericide and anti-inflammatory activity in human colon cancer cells. BMC Complement Altern Med 18: 202, 2018.
16. Suzui M: An anticancer agent derived from natural fatty acid. Chemical Industry 66: 22-27, 2015 (In Japanese).
17. Suzui M and Iinuma M: Anticancer agent. Japan Patent. No. 5597427, 2014.
18. Suzui M, Masuda M, Lim JTE, Albanese C, Pestell RG and Weinstein IB: Growth inhibition of human hepatoma cells by acyclic retinoid is associated with induction of p21(CIP1) and inhibition of expression of cyclin D1. Cancer Res 62: 3997-4006, 2002.
19. Suzui M, Inamine M, Kaneshiro T, Morioka T, Yoshimi N, Suzuki R, Kohno H and Tanaka T: Indole-3-carbinol inhibits the growth of human colon carcinoma cells but enhances the tumor multiplicity and volume of azoxymethane-induced rat colon carcinogenesis. Int J Oncol 27: 1391-1399, 2005.
20. Suzui M, Sunagawa N, Chiba I, Moriwaki H and Yoshimi N: Acyclic retinoid, a novel synthetic retinoid, induces growth inhibition, apoptosis, and changes in mRNA expression of cell cycle- and differentiation-related molecules in human colon carcinoma cells. Int J Oncol 28: 1193-1199, 2006.
21. Suzui M, Shimizu M, Masuda M, Lim JTE, Yoshimi N and Weinstein IB: Acyclic retinoid activates retinoic acid receptor beta and induces transcriptional activation of p21(CIP1) in HepG2 human hepatoma cells. Mol Cancer Ther 3: 309-316, 2004.
22. Kawamori T, Rao CV, Seibert K and Reddy BS: Chemopreventive activity of celecoxib, a specific cyclooxygenase-2 inhibitor, against colon carcinogenesis. Cancer Res 58: 409-412, 1998.
23. Futakuchi M, Nitanda T, Ando S, Matsumoto H, Yoshimoto E, Fukamachi K and Suzui M: Therapeutic and preventive effects of osteoclastogenesis inhibitory factor on osteolysis, proliferation of mammary tumor cell and induction of cancer stem cells in the bone microenvironment. Int J Mol Sci 19: 888, 2018.
24. Suzui M, Morioka T and Yoshimi N: Colon preneoplastic lesions in animal models. J Toxicol Pathol 26: 335-341, 2013.
25. Bird RP: Observation and quantification of aberrant crypts in the murine colon treated with a colon carcinogen: preliminary findings. Cancer Lett 37: 147-151, 1987.

26. Kanda Y: Investigation of the freely available easy-to-use software 'EZR' for medical statistics. Bone Marrow Transplant 48: 452-458, 2013.
27. Yu H and Jove R: The STATs of cancer-new molecular targets come of age. Nat Rev Cancer 4: 97-105, 2004.
28. Lin Q, Lai R, Chirieac LR, Li C, Thomazy VA, Grammatikakis I, Rassidakis GZ, Zhang W, Fujio Y, Kunisada K, *et al*: Constitutive activation of JAK3/STAT3 in colon carcinoma tumors and cell lines: Inhibition of JAK3/STAT3 signaling induces apoptosis and cell cycle arrest of colon carcinoma cells. Am J Pathol 167: 969-980, 2005.
29. Shuai K, Horvath CM, Huang LH, Qureshi SA, Cowburn D and Darnell JE Jr: Interferon activation of the transcription factor Stat91 involves dimerization through SH2-phosphotyrosyl peptide interactions. Cell 76: 821-828, 1994.
30. Weinstock LT, Rost WJ and Cheng CC: Synthesis of new polyamine derivatives for cancer chemotherapeutic studies. J Pharm Sci 70: 956-959, 1981.
31. Carpenter RL and Lo HW: STAT3 target genes relevant to human cancers. Cancers 6: 897-925, 2014.
32. Reich NC and Liu L: Tracking STAT nuclear traffic. Nat Rev Immunol 6: 602-612, 2006.
33. Fletcher S, Turkson J and Gunning PT: Molecular approaches towards the inhibition of the signal transducer and activator of transcription 3 (Stat3) protein. Chem Med Chem 3: 1159-1168, 2008.
34. Pfeffer CM and Singh ATK: Apoptosis: A target for anticancer therapy. Int J Mol Sci 19: 448, 2018.
35. Lin L, Hutzen B, Li PK, Ball S, Zuo M, DeAngelis S, Foust E, Sobo M, Friedman L, Bhasin D, *et al*: A novel small molecule, LLL12, inhibits STAT3 phosphorylation and activities and exhibits potent growth-suppressive activity in human cancer cells. Neoplasia 12: 39-50, 2010.
36. Song H, Wang R, Wang S and Lin J: A low-molecular-weight compound discovered through virtual database screening inhibits Stat3 function in breast cancer cells. Proc Natl Acad Sci USA 102: 4700-4705, 2005.
37. Baum O, Suter F, Gerber B, Tschanz SA, Buergy R, Blank F, Hlushchuk R and Djonov V: VEGF-A promotes intussusceptive angiogenesis in the developing chicken chorioallantoic membrane. Microcirculation 17: 447-457, 2010.
38. Fenoglio-Preiser CM and Noffsinger A: Aberrant crypt foci: A review. Toxicol Pathol 27: 632-642, 1999.
39. Di Gregorio C, Losi L, Fante R, Modica S, Ghidoni M, Pedroni M, Tamassia MG, Gafà L, Ponz de Leon M and Roncucci L: Histology of aberrant crypt foci in the human colon. Histopathology 30: 328-334, 1997.
40. Nucci MR, Robinson CR, Longo P, Campbell P and Hamilton SR: Phenotypic and genotypic characteristics of aberrant crypt foci in human colorectal mucosa. Hum Pathol 28: 1396-1407, 1997.
41. Shpitz B, Bomstein Y, Mekori Y, Cohen R, Kaufman Z, Neufeld D, Galkin M and Bernheim J: Aberrant crypt foci in human colons: Distribution and histomorphologic characteristics. Hum Pathol 29: 469-475, 1998.